

# Metalorganic chemical vapor deposition of highly oriented thin film composites of $V_2O_5$ and $V_6O_{13}$ : Suppression of the metal–semiconductor transition in $V_6O_{13}$

M.B. Sahana and S.A. Shivashankar<sup>a)</sup>

Materials Research Centre, Indian Institute of Science, Bangalore-560 012, India

(Received 19 November 2003; accepted 3 May 2004)

Thin films of vanadium oxides were grown on fused quartz by metalorganic chemical vapor deposition using vanadyl acetylacetonate as the precursor. Growth at temperatures  $\geq 560$  °C results in composites of strongly (00 $l$ )-oriented  $V_2O_5$  and  $V_6O_{13}$ . The dominant phase of the film changes from  $V_2O_5$  to  $V_6O_{13}$ , and back to  $V_2O_5$ , as the growth temperature is raised from 560 to 570 °C, then to 580 °C, as evidenced by x-ray diffraction and Rutherford backscattering analyses. This reentrant-type growth trend was interpreted on the basis of the small difference in the free energy of formation of  $V_2O_5$  and  $V_6O_{13}$  and the presence of metal–oxygen bonds in the precursor. In contrast with single-crystalline  $V_6O_{13}$ , the film predominantly composed of highly oriented single-crystalline platelets of  $V_6O_{13}$  did not undergo the semiconductor–metal transition at  $-123$ ° K, despite the connectivity being well above the percolation threshold. Instead, a semiconductor-to-semiconductor transition was observed in this film, which is explained in terms of the observed relaxation of the edges of all the platelets of metallic  $V_6O_{13}$  to semiconducting  $V_2O_5$ .

## I. INTRODUCTION

The vanadium oxide system is rich and interesting because of the diversity of physical properties observed in apparently similar phases. For example, while vanadium pentoxide is a wide band gap semiconductor,<sup>1</sup>  $V_6O_{13}$ , which has a very similar structure, is a metal at room temperature.  $V_6O_{13}$  undergoes a metal–semiconductor (M-S) transition at  $-123$ ° C, with a jump in resistivity by a factor of  $10^5$ , though this is observed only in single-crystalline specimen.<sup>2</sup> Sintered polycrystalline  $V_6O_{13}$ , by contrast, is reported to be a semiconductor at room temperature<sup>3</sup> with activation energy for conduction  $E_a$  of 0.42 eV. It exhibits a semiconductor-to-semiconductor (S-S) transition<sup>3</sup> at approximately 150 K, where the resistivity jumps by about an order of magnitude, the  $E_a$  at low temperatures being 0.21 eV. The M-S transition is accompanied by a crystallographic distortion.<sup>4</sup> Furthermore, an antiferromagnetic ordering<sup>5</sup> takes place in  $V_6O_{13}$  at 50 K. While  $V_2O_5$  is thermodynamically stable, the  $V_6O_{13}$  phase, being an ordered defect structure closely related to  $V_2O_5$ , is metastable. Although accurate thermodynamic data ( $\Delta G$ , the Gibbs free energy of formation) are not available for

$V_6O_{13}$ , it may be expected from the V–O binary phase diagram<sup>6</sup> that the free energy of  $V_6O_{13}$  is likely to be close to that of  $V_2O_5$ . This is substantiated by the present study and is understandable given the intimate relationship between the crystal structures of  $V_2O_5$  and  $V_6O_{13}$ . The  $V_2O_5$  lattice in the  $c$  direction can be considered as stacking of alternately pure vanadyl oxygen (O) and mixed vanadium oxygen (V–O) layers [Fig. 1(a)]. Along the  $c$  axis, each vanadyl oxygen is bonded to two vanadium atoms, in one direction by a double bond and in the opposite direction by a van der Waals bond. The successive O and V–O layers are kept together by an equal number of weak van der Waals bonds and much stronger double bonds.<sup>7</sup> The crystal structure of  $V_6O_{13}$  can be deduced from the  $V_2O_5$  stacking by removing each third O layer and successive shear over  $1/6[10\bar{3}]$ . The resulting stacking sequence<sup>8</sup> is of the form . . . O, V–O, O, V–O, O, V–O, V–O . . . [Fig. 1(b)]. It should be noted that in  $V_6O_{13}$  the bonding between the pure O layers and V–O layers is of neither the vanadyl nor the van der Waals type. However,  $V_2O_5$  and  $V_6O_{13}$  have similar polyhedral connectivity and a similar two-dimensional repeat unit along the  $a$ - $b$  plane [Figs. 1(c) and 1(d)]; the unit cell of the  $V_2O_5(001)$  surface is  $11.52 \times 3.56$  Å, and that of  $V_6O_{13}(001)$  surface is  $11.92 \times 3.68$  Å. The  $a$ - $b$  planes of both  $V_2O_5$  and  $V_6O_{13}$  are made up of a network of corner sharing zig-zag strings consisting of edge-shared polyhedra, forming closely packed dense planes.<sup>6</sup>

<sup>a)</sup>Address all correspondence to this author.

e-mail: shivu@mrc.iisc.ernet.in

DOI: 10.1557/JMR.2004.0394

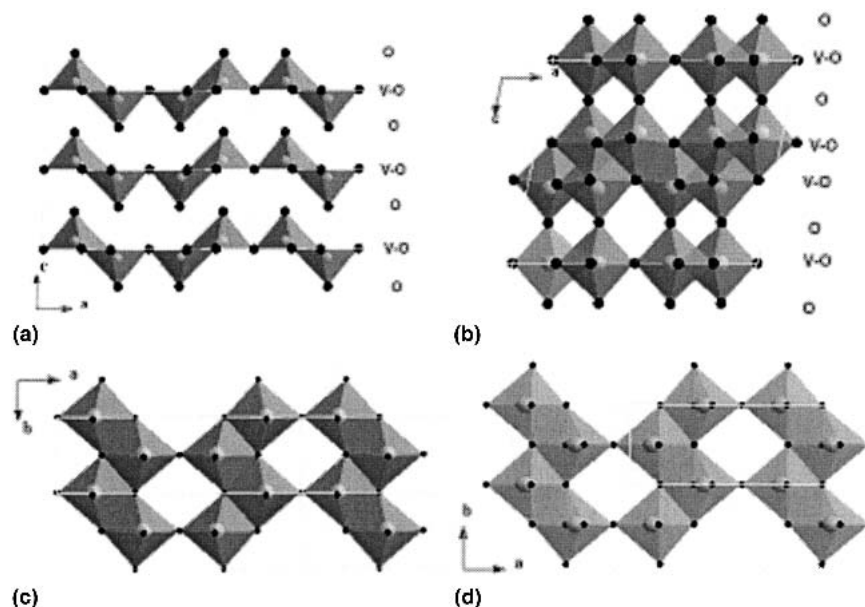


FIG. 1. The arrangement of oxygen polyhedra in the  $(ac)$  plane, depicting the stacking sequences of O and V-O layers in (a)  $V_2O_5$ , (b)  $V_6O_{13}$ , and in the  $(ab)$  plane in (c)  $V_2O_5$  and (d)  $V_6O_{13}$ .

Moreover, both  $V_2O_5$  and  $V_6O_{13}$  are technologically important.  $V_2O_5$  has been widely studied as a promising material for a variety of applications: as a catalyst,<sup>9,10</sup> a gas sensor,<sup>11</sup> a window material for solar cells, in electrochemical devices,<sup>12</sup> as a cathode material for solid-state batteries.<sup>13</sup> Theoretical studies predict that the orientation of  $V_2O_5$  has a great influence on Li-ion transport across the electrolyte/cathode interface in solid-state thin film batteries or electrochromic devices (cyclic stability and reversibility).<sup>14</sup> Fang et al. have reported that the  $(00l)$  orientation of  $V_2O_5$  improves cycle stability of Li-ion intercalation and de-intercalation and its reversibility.<sup>15</sup> For this reason, different deposition techniques such as pulsed laser deposition,<sup>15,16</sup> plasma-enhanced chemical vapor deposition (PECVD),<sup>17</sup> atmospheric pressure chemical vapor deposition (CVD),<sup>18</sup> and vacuum evaporation,<sup>19,20</sup> have been explored to grow oriented  $V_2O_5$  films. Similarly,  $V_6O_{13}$  has also been studied extensively as a candidate cathode material in solid-state lithium-ion batteries.<sup>21,22</sup> As  $V_6O_{13}$  has a structure similar to that of  $V_2O_5$ , it appears that  $(00l)$ -orientated  $V_6O_{13}$  films would also be interesting as intercalation hosts for Li ions in rechargeable batteries and electrochromic devices, just as  $(00l)$ -oriented  $V_2O_5$ . However, there are very few reports on thin films of  $V_6O_{13}$  and, in particular, on oriented  $V_6O_{13}$  thin films.<sup>23,24</sup> To exploit the potential of these two materials fully, a further understanding of the dependence of phase formation, crystallinity, and orientation of the film on deposition parameters is required, because of the close relationship between the structures of the two oxides. In our recent effort to investigate the metalorganic CVD

(MOCVD) of vanadium oxide thin films using vanadyl acetylacetonate,  $VO(acac)_2$ , as the precursor, we have observed that highly oriented films of different phases such as  $VO_2(B)$ ,  $VO_2(M)$ , and  $\beta-Na_xV_2O_5$  can be obtained by varying process parameters.<sup>25-27</sup> It is also found that the phase formed, microstructure, orientation, and the crystallinity of the film change significantly, even within a narrow range of growth temperatures.<sup>25-27</sup>

In this study, we have therefore grown thin films of vanadium oxides on fused quartz by MOCVD using  $VO(acac)_2$  as the precursor, at various temperatures from 550 to 610 °C. The phase formed and the microstructure of the films were examined as a function of deposition temperature. It is observed that, as the temperature is varied from 560 to 580 °C in steps of 10 °C, the films deposited comprise a mixture of strongly oriented  $V_2O_5$  and  $V_6O_{13}$  phases, with the x-ray diffraction (XRD) patterns being alternately dominated by either  $V_6O_{13}$  or  $V_2O_5$ . Indeed, films grown at various temperatures >550 °C have a strong tendency for the  $(00l)$  texture, irrespective of the dominant phase. Such reentrant-type behavior in phase formation has not been reported to date and is interpreted here through suitably designed experiments. Further, it is found that the film predominantly comprised of highly oriented  $V_6O_{13}$  does not undergo the S-M transition at 150 K. This is explained on the basis of the observed relaxation of the edges of  $V_6O_{13}$  crystallites into the thermodynamically more stable  $V_2O_5$  phase. This argument is further extended to explain the reported absence of S-M transition in the polycrystalline samples of  $V_6O_{13}$ .

## II. EXPERIMENTAL

Thin films of composites of  $V_2O_5$  and  $V_6O_{13}$  were grown on polished fused quartz substrates (measuring approximately  $10\text{ mm} \times 10\text{ mm}$ ) by low pressure MOCVD in a hot-wall, horizontal reactor built in house, using vanadyl acetylacetonate  $[VO(acac)_2]$  as the precursor. This precursor, a crystalline solid that sublimates beginning at approximately  $150\text{ }^\circ\text{C}$ , was synthesized in our laboratory and purified by repeated recrystallization. A detailed description of the CVD system and the thermal analysis of  $VO(acac)_2$  are given elsewhere.<sup>25</sup> The precursor was vaporized at  $175\text{ }^\circ\text{C}$ , while high-purity argon was used as the carrier gas, and high purity oxygen as the oxidant gas. Gas flow was regulated using electronic mass flow controllers. A relatively high flow rate of oxygen (350 sccm) was used, compared to that of argon (60 sccm), in the expectation that vanadium oxide films might be formed, in which at least some of the vanadium would be in the 5+ state. A capacitance manometer was used to measure the total reactor pressure, which was maintained at 100 Torr. The films were deposited for 2 h, at different temperatures in the range  $550$  to  $610\text{ }^\circ\text{C}$ . The exact temperature of the substrate was measured using a K-type thermocouple inserted into the susceptor, on which the substrate was placed. At the end of each deposition, power supply to the reactor was turned off, thus allowing the samples to cool to room temperature in an ambient of flowing oxygen (350 sccm). Some of the samples were subjected to post-deposition annealing for various durations in flowing oxygen, at the temperature of deposition of the given sample.

Identification of the phases present in the films was carried out using powder XRD (Scintag 2000 diffractometer,  $\text{Cu K}_\alpha$  radiation). To determine film composition, some of the samples were analyzed by Rutherford backscattering spectrometry (RBS), employing 2.4 MeV alpha particles in a 3 MV tandem accelerator (HVEE, Europa, Amsterdam, Holland). A well-collimated beam (spot size  $<0.5\text{ mm}$ ) of alpha particles was incident normal to the specimens, and the backscattered particles were detected by a silicon surface barrier detector positioned at  $170^\circ$  with respect to the direction of the incident beam.

The microstructure of the films was examined by scanning electron microscopy (SEM; JEOL Model JSM-5600LV, Tokyo, Japan) and transmission electron microscopy (TEM; JEOL model JEM 200CX, Tokyo, Japan). Film thickness was measured using cross-sectional SEM micrographs. TEM samples were prepared by scraping the film out of the substrate and dripping it using acetone onto a carbon-coated copper grid. The resistance of the film mainly comprising  $V_6O_{13}$  was measured by the linear four-probe method from  $20$ – $300\text{ K}$  in a closed-cycle cryostat, during both the cooling and heating cycles. The optical properties of the films grown at different temperatures were studied by recording their

transmittance in the ultraviolet-visible (UV-vis) region in a scanning spectrophotometer (Shimadzu, double beam, resolution  $0.1\text{ nm}$ ).

## III. RESULTS

Films deposited on fused quartz at various temperatures in the range  $550$  to  $610\text{ }^\circ\text{C}$  are designated as VT, where T gives the temperature in degrees celsius. XRD patterns of these films are given in Fig. 2 and are indexed according to the standard powder patterns for polycrystalline, orthorhombic  $V_2O_5$ , tetragonal  $V_4O_9$ , and monoclinic  $V_6O_{13}$  (JCPDS file Nos. 41-1426, 23-0720, and 43-1050, respectively).<sup>28</sup> The film V550 is a mixture of the phases  $V_2O_5$ ,  $V_6O_{13}$ , and  $V_4O_9$ , with no tendency for preferred orientation. The peak intensities are very low, even though the film is quite thick (Table I) and well crystallized, as is evident from the SEM shown below [Fig. 3(a)]. The broad hump in the range  $2\theta = 15^\circ$  to  $30^\circ$  is due to the underlying fused quartz substrate. By contrast, this hump is inconspicuous in the XRD pattern of the films grown at temperatures  $>550\text{ }^\circ\text{C}$  because of the much higher intensities (by more than an order of magnitude) of the reflections arising from the pronounced (001) orientation of either or both of the phases,  $V_2O_5$  and  $V_6O_{13}$ , present in these films. (The presence of  $V_4O_9$ , if any, in the films grown at temperatures  $>550\text{ }^\circ\text{C}$  is below the limit of detection of XRD.) For example, in the XRD

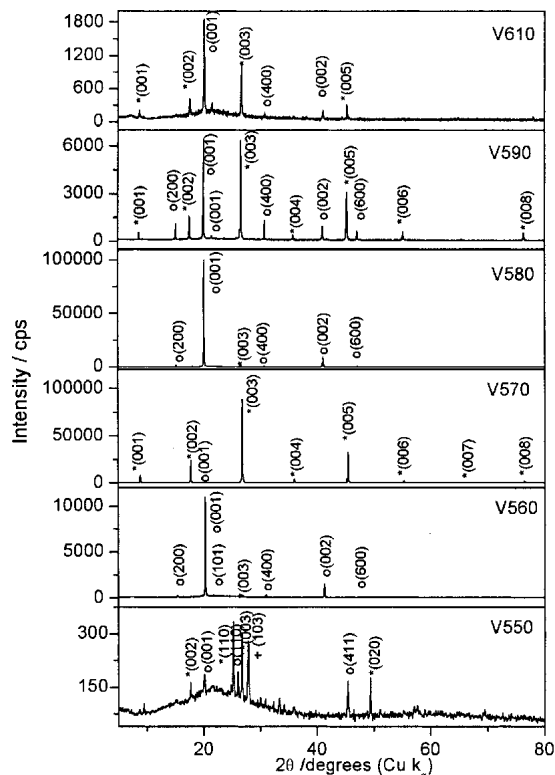


FIG. 2. XRD patterns of the films grown at various temperatures in the range  $550$  to  $610\text{ }^\circ\text{C}$ : (\*)  $V_6O_{13}$ , (o)  $V_2O_5$ , and (+)  $V_4O_9$ .

TABLE I. Phase content, oxygen-to-vanadium ratio, color in transmission, and thickness of films grown at different temperatures for 2 h; bold font designates the phase dominating the XRD pattern

Sample designation	Phase content	Color in transmission	Film thickness (nm)	Oxygen to vanadium ratio from RBS data	$V_2O_5:V_6O_{13}$ (mol%) calculated from RBS data
V550	$V_2O_5$ , $V_6O_{13}$ , $V_4O_9$	Opaque	1530		
V560	<b><math>V_2O_5</math></b> , $V_6O_{13}$	Yellow	450	2.45	85:15
V570	$V_2O_5$ , <b><math>V_6O_{13}</math></b>	Brownish black	500	2.2	12:88
V580	<b><math>V_2O_5</math></b> , $V_6O_{13}$	Pinkish yellow	1250	2.3	41:59
V590	$V_2O_5$ , $V_6O_{13}$	Brown + yellow	1200		
V610	$V_2O_5$ , $V_6O_{13}$	Sparse coating	300		

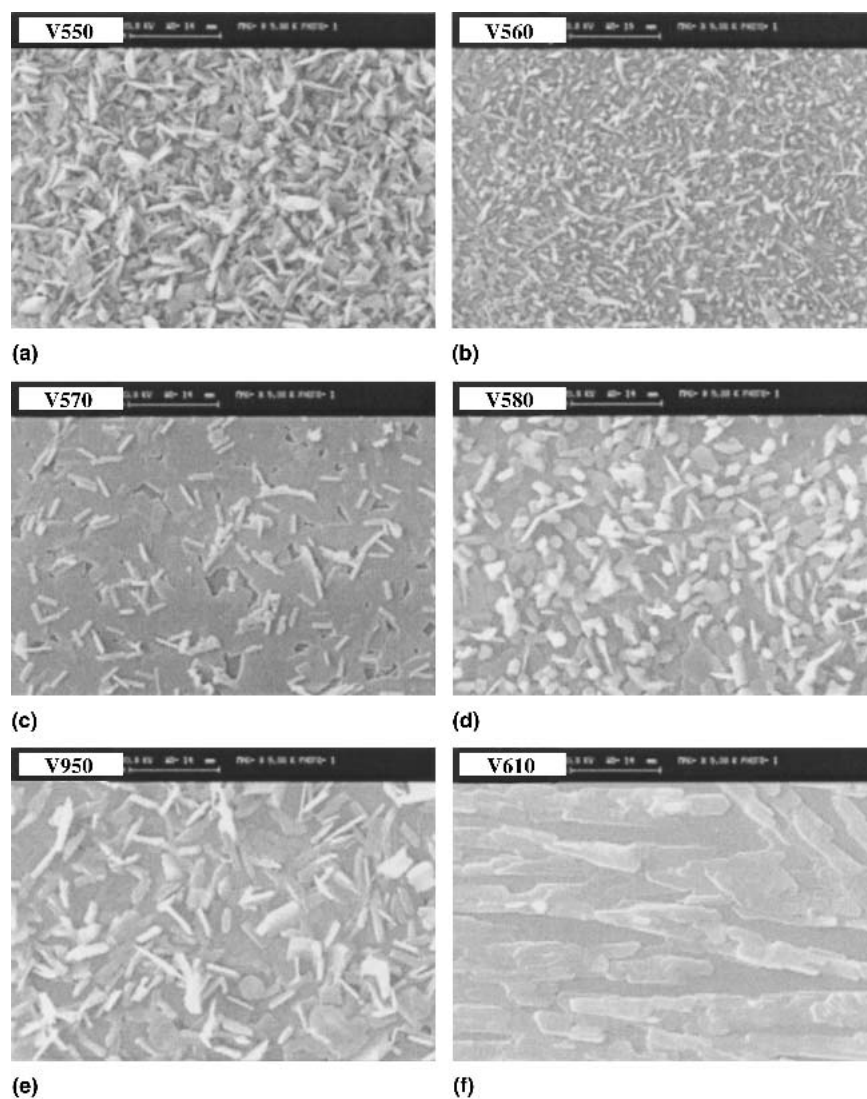


FIG. 3. SEM micrographs of the films grown at various temperatures: (a) 550 °C, (b) 560 °C, (c) 570 °C, (d) 580 °C, (e) 590 °C, and (f) 610 °C.

pattern of V560, the intensity of the (00 $l$ ) reflections of  $V_2O_5$ , in comparison with that of the other peaks, is very high. Even though the (00 $l$ ) peak is the strongest reflection in the polycrystalline powder pattern of  $V_2O_5$ , the intensity ratio ( $I_{(001)}/I_{(hkl)}$ ) in V560 is much higher than it would be in polycrystalline  $V_2O_5$ , indicating growth with a strong (00 $l$ ) texture. The simultaneous deposition of

$V_6O_{13}$  in V560 is evidenced by the low intensity peak at  $2\theta = 26.8^\circ$  seen in the XRD pattern. However, it must be noted that the preferred orientation of  $V_2O_5$  in the film prevents an estimation (using XRD data) of the relative proportion of the two oxide phases in V560. When the deposition temperature is 570 °C, the XRD pattern of the resulting film is dominated by  $V_6O_{13}$ , with peak

intensities higher by an order of magnitude than in V560. The presence of only the (00 $l$ ) reflections indicates that V570 is a film of  $V_6O_{13}$  with a strong (00 $l$ ) texture. However, the (001) peak of  $V_2O_5$  observed in V570 remains in the film V560, though its intensity is sharply reduced. When deposition is carried out at 580 °C, the dominant reflection is due to  $V_2O_5$ , which has a strongly preferred (00 $l$ ) orientation, just as in V560, but with a further increase in the intensity of the (001) peak. It should be noted that the intensities of the XRD peaks due to  $V_6O_{13}$  and  $V_2O_5$  from V570 and V580, respectively, are comparable to the intensities of the peaks observed from an epitaxial film grown on a single crystal substrate. The formation of films containing highly oriented grains of both  $V_2O_5$  and  $V_6O_{13}$ , each phase dominating the other by turn when the deposition temperature is varied within the very narrow range from 560 to 580 °C, has been confirmed by repeated growth runs. When the growth temperature is increased again by 10 °C to 590 °C, the resulting film continues to be a mixture of  $V_2O_5$  and  $V_6O_{13}$ , both with a pronounced (00 $l$ ) texture. However, in this film (V590), the intensities of the peaks due to  $V_2O_5$  and  $V_6O_{13}$  are comparable, neither dominating the other, in contrast with films grown at lower temperatures. Furthermore, the intensity of the XRD peaks in V590 is lower by more than an order of magnitude than in V570 and V580. As the growth temperature is raised further to 610 °C, the resulting film is again comprised of (00 $l$ )-oriented  $V_2O_5$  and  $V_6O_{13}$ , with peak intensities comparable to each other. But, the intensity of the pattern is smaller still than that of V590. Thus, over a narrow range of deposition temperatures, strongly textured growth of a thin film composite of  $V_2O_5$  and  $V_6O_{13}$  is observed. As a function of deposition temperature in the range 560–580 °C, each of the two oxide phases dominates the other alternately in the XRD patterns of these composite films. This may be termed as reentrant-type behavior in the growth of vanadium oxide films under the MOCVD conditions used here.

A measurement of the oxygen content of these films is, therefore, pertinent. The phase content, the oxygen-to-vanadium ratio, color in transmission, and the thickness of the films grown at different temperatures (for 2 h) are summarized in Table I. It is noteworthy that V560 and V570 have a similar thickness, but much smaller than that of V550, V580, or V590. As two or more phases are being deposited simultaneously, no Arrhenius-type dependence of growth rate on temperature, typical of CVD processes, may be expected.<sup>25,27</sup> It is also to be noted that the oxygen content of the films V560, V570, and V580, as analyzed by RBS, has an accuracy of 5%. A reason for this (relatively) low accuracy is the absence of a sharp interface between the film and substrate. Given the limited accuracy of the RBS analysis, it is not possible to determine very reliably the relative proportions of the

two phases present in the film. Within these limitations, the percentages of  $V_2O_5$  and  $V_6O_{13}$  present in V560, V570, and V580, as estimated from RBS data, are listed in Table I. It is to be noted that these values are quite sensitive to the O:V assumed in the estimations. For example, assuming that the error in RBS analysis is as low as 2%—i.e., when O:V =  $2.45 \pm 0.05$ —the relative proportion of  $V_2O_5$  and  $V_6O_{13}$  lies within a band of 100:0 (when O:V ratio is taken to be 2.50) to 70:30 (when O:V ratio is 2.40). This illustrates the difficulty in determining experimentally the proportions of two such compositionally close phases comprising a thin film sample. Nevertheless, the variation in the measured oxygen content of the films with the deposition temperature supports the inference from XRD data that reentrant-type growth occurs in the MOCVD of higher vanadium oxides.

Because of the observed curious progression in the XRD patterns of the films deposited over a narrow range of temperatures, the microstructure of the films was examined by scanning electron microscopy. It is found that the microstructure varies significantly with deposition temperature, as manifested in the SEM micrographs shown in Fig. 3. However, all the films except for V550 share a common feature; i.e., they consist of two types of crystallites with different levels of contrast, the relative proportion of the two types varying with the growth temperature. It is well known that semiconductors and insulators appear brighter in SEM micrographs than metals, because of the lower rates of charge leakage. Based on the XRD data presented, and the SEM micrographs [Figs. 3(b)–3(e)], it may be concluded that the films grown at temperatures between 560 and 590 °C consist of a non-conducting phase ( $V_2O_5$ ) and a conducting phase ( $V_6O_{13}$ ), whose relative proportion appears to vary with the growth temperature, as verified by RBS analysis (Table I).

It may be seen from Fig. 3(a) that the film V550 is well crystallized and the crystallites are large, measuring up to 2  $\mu\text{m}$  in extension, with many of them being platelets of different shapes. We surmise that the observed microstructure is due to the simultaneous deposition of three different oxide phases. The film V560, by contrast, comprises only two phases, i.e.,  $V_2O_5$  (the bright crystallites), and  $V_6O_{13}$  (the darker crystallites). Nevertheless, crystallite size, as well as crystallite shape, covers a wide range, as can be readily noted from Fig. 3(b). Indeed, a thin “ribbon”—ostensibly of  $V_2O_5$ , because of its brightness—near the center of the micrograph measures as much as 5  $\mu\text{m}$ . On the other hand, V570 is made of large, dark platelets, presumably of  $V_6O_{13}$ , lying parallel to the substrate surface [Fig. 3(c)]. Given the high intensity of the XRD pattern, we infer that V560 is composed of single-crystalline platelets of  $V_6O_{13}$ , some measuring more than 25  $\mu\text{m}$  across. On these dark platelets is seen a random and sparse “sprinkling” of bright crystallites.

Because the XRD pattern of V570 consists of a minute peak corresponding to  $V_2O_5$ , we hypothesize that the small, bright crystallites dispersed over the large platelets are those of  $V_2O_5$ . By contrast, the SEM of the film V580 [Fig. 3(d)] reveals it to be an intimate composite of bright and dark crystallites, which may be inferred as those of  $V_2O_5$  and  $V_6O_{13}$ , respectively. The crystallites of  $V_2O_5$  are highly faceted, suggesting that growth (of  $V_2O_5$ ) occurs at this temperature under close-to-equilibrium conditions. It is also to be noted that the crystallites of  $V_6O_{13}$  are much smaller, and are no longer the large platelets that nearly cover the entire substrate as in V570. As evident from Fig. 3(e), V590 is also composed of two types of crystallites, i.e.,  $V_2O_5$  and  $V_6O_{13}$ , both with a preference for the (001) orientation, and in comparable proportion. The average size of the crystallites is larger than in V580, though they are faceted to a lesser degree. As the deposition temperature is raised to 610 °C, the rate of deposition falls sharply, resulting in a much thinner "film." Indeed, the coating is very sparse on the substrate and is made of branched, interconnected platelets parallel to the substrate, with a continuously changing contrast in the SEM [Fig. 3(f)], suggesting intergrowth of  $V_2O_5$  and  $V_6O_{13}$ .

As the films grown at different temperatures are shown by XRD and SEM to be composites of  $V_2O_5$  and  $V_6O_{13}$ , respectively a semiconductor and a metal, their optical transmittance was examined as a function of wavelength. The transmittance of V560, V570, and V590 are shown in Fig. 4. The transmittance of V560 is a very gradually increasing function of wavelength, reaching a maximum of approximately 35% at 1000 nm, whereas V570 has a peak transmittance of approximately 8% at 540 nm. The film V590 is poorly transmitting, reaching a maximum of only 5% at 1000 nm, but with an inflexion at 540 nm, presumably corresponding to the wavelength of maximum transmission in V570. The composite nature of the films renders the estimation of the respective band gap from a plot of  $\alpha^2$  versus  $h\nu$  difficult. Nevertheless, a value of 2.0 eV may be estimated for the  $V_2O_5$  component of V590, which is in good agreement with the reported band gap<sup>29</sup> of single crystals of  $V_2O_5$ .

The selected-area diffraction (SAED) pattern of one of the large platelets of  $V_6O_{13}$  in V570, taken along (002) is shown in Fig. 5. Also shown in the figure is the SAED pattern of a well-faceted crystallite of  $V_2O_5$  from V580, taken along (002). It is clear from the SAED patterns that  $V_6O_{13}$  and  $V_2O_5$  have a very similar structure in the  $a$ - $b$  plane. (That the latter pattern is due to  $V_2O_5$  was verified by obtaining identical SAED patterns from a number of crystallites in  $V_2O_5$  with different, strongly faceted morphologies, which constitute V580.)

As single crystals of  $V_6O_{13}$  have been shown to undergo (upon cooling) a M-S transition at 150 K, a temperature-dependent resistance measurement of the

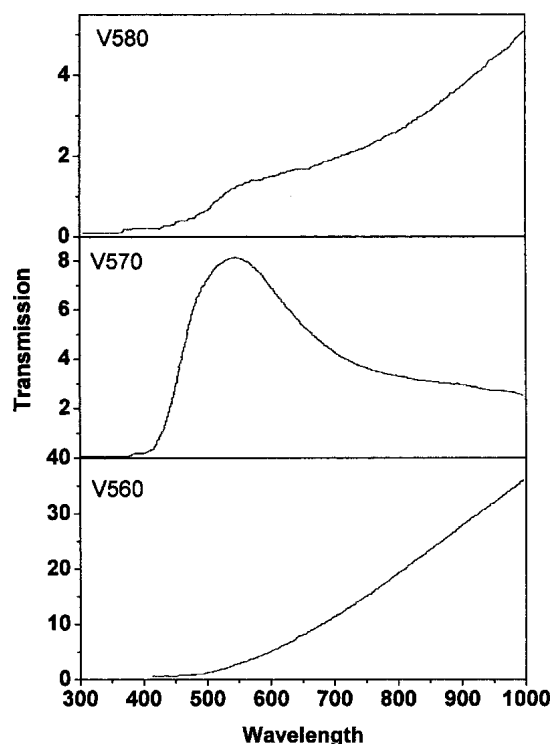


FIG. 4. Transmittance spectra of V560, V570, and V590.

film V570 consisting predominantly of  $V_6O_{13}$ , was carried out. The Arrhenius plot of resistance versus temperature is given in Fig. 6. Curiously, even though the film is composed of large, well connected, single-crystalline platelets of  $V_6O_{13}$ , no evidence of a S-M transition within the temperature range 20–300 K is observed. The film is found to be semiconducting throughout this temperature range, with a change in slope in the Arrhenius plot at about 125 K. While conduction from 300 to 125 K is characterized by an activation energy of 0.07 eV, conduction at lower temperatures has a complex dependence on temperature. Even though there is no report of electrical measurements on thin films of  $V_6O_{13}$ , the temperature dependence of the conductivity of polycrystalline V570 (though strongly oriented) may be expected to be similar to that of polycrystalline  $V_6O_{13}$ . However, unlike a sintered polycrystalline pellet of  $V_6O_{13}$ , the film V570 does not display any discontinuity in resistance at any temperature. The absence of a M-S transition at 150 K, i.e., a jump in conductivity at ~150 K in the film V570, is puzzling because it is composed of relatively large, single-crystalline platelets of  $V_6O_{13}$ , all of them aligned with the  $a$ - $b$  plane parallel to the substrate surface, and apparently well connected; indeed, the connectivity, as observed through SEM, is well above the percolation threshold.

To unravel these intriguing features, a closer examination of the film V570 was undertaken. In particular,

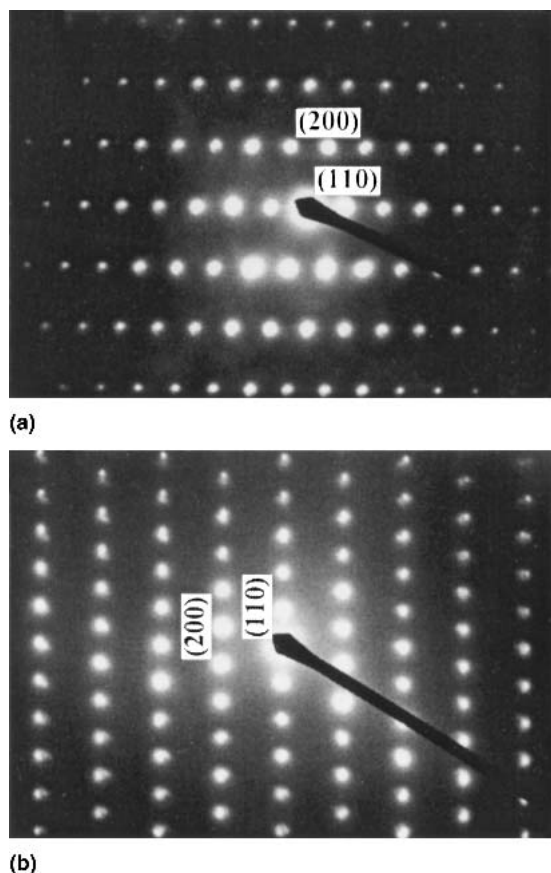


FIG. 5. SAED pattern of (a)  $V_6O_{13}$  and (b)  $V_2O_5$ , taken along [002].

SEM analysis of the film was carried out at higher resolution. The SEM image of a segment of V570 is shown in Fig. 7. It may be seen that where two platelets of  $V_6O_{13}$  meet each other such that the edges of the platelets are “exposed,” the contrast of the image is very high: the edges are distinctly much brighter than the “inner” segments of the platelets. This suggests that the edges of the platelets might indeed be made of  $V_2O_5$ , a large band gap semiconductor, accounting for the contrast in the SEM image. It was found by detailed SEM analysis that, at every location in V570 where platelets of  $V_6O_{13}$  meet, the edges of the platelets exhibit a sharp contrast in brightness with the “inner” portions of the platelets, suggesting the edges of all (single crystalline) platelets of  $V_6O_{13}$  had been transformed into  $V_2O_5$ . (It was verified that the contrast in the SEM images was not an artifact of the orientation of the specimen relative to the electron beam.)

Prompted by this observation, transmission electron microscopy was used to examine the edges of the platelets in V570. Two TEM bright-field images of a large platelet of  $V_6O_{13}$  in V570, one taken at its center and the other at one edge, are given in Fig. 8, together with the corresponding SAED patterns taken along (002). Three boundaries and dislocation fringes are seen vividly at the

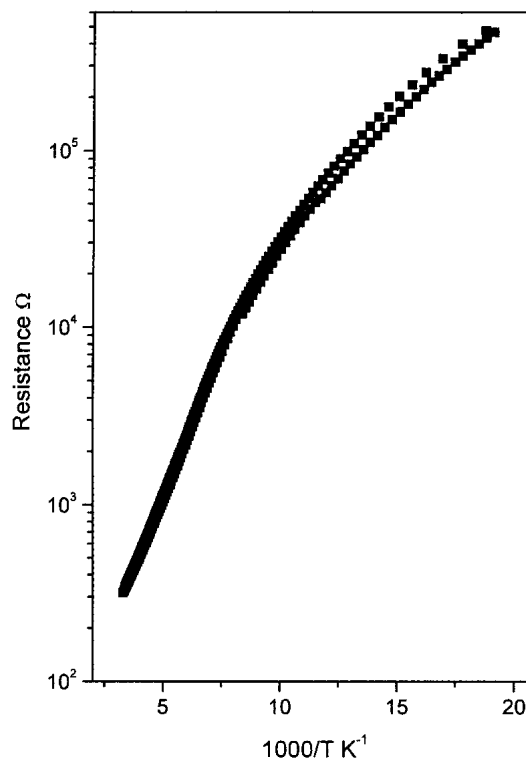


FIG. 6. Arrhenius plot of resistance of the film V570.

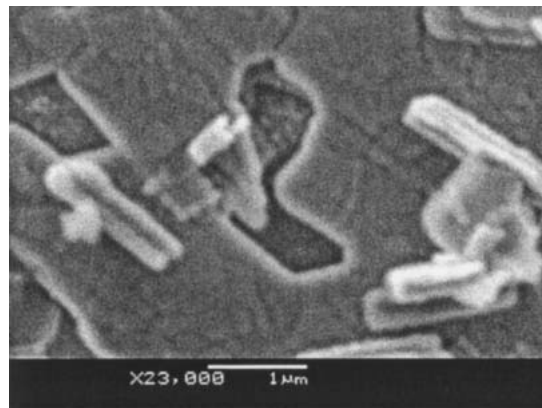


FIG. 7. SEM image of a segment of V570 at higher resolution, showing the brightness contrast between the edges and the interior of platelets.

edge [Fig. 8(c)], in contrast with the smooth interior of the platelet [Fig. 8(a)]. Further, the corresponding SAED patterns show large differences between the two regions of the platelet. The diffraction pattern of the center of the platelet is single crystalline [Fig. 8(b)]. Multiple reflections are observed at the edge [Fig. 8(d)], possibly from two or more phases present at the edge and from double diffraction (i.e., from diffraction in addition to that attributable to  $V_6O_{13}$ ).

To investigate further the formation of the  $V_2O_5$  phase at the edges of  $V_6O_{13}$  crystals, the films V560, V570, and V580 were annealed in flowing oxygen at the deposition

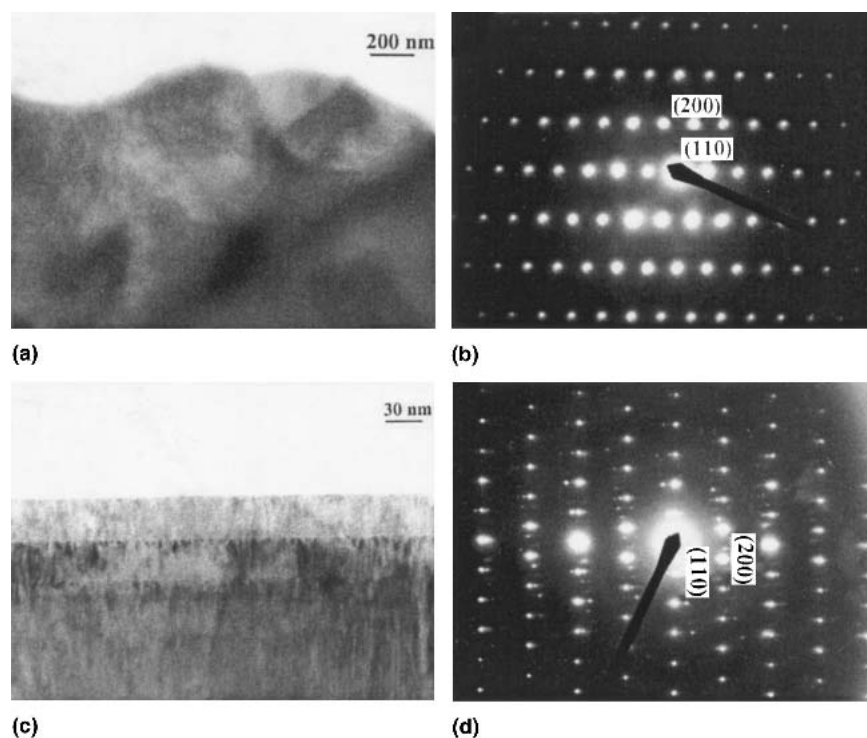


FIG. 8. TEM bright-field image and the corresponding SAED pattern taken along (002) of one of the larger platelets of  $V_6O_{13}$  in V570: (a,b) interior of the platelet, (c,d) edge of the platelet.

temperature. It is observed that the  $V_6O_{13}$  phase in the films V560 and V580, whose XRD patterns were dominated by  $V_2O_5$ , converts completely to  $V_2O_5$  after 20 min of annealing. However, in the sample, V570, which is dominated by  $V_6O_{13}$ , complete conversion to  $V_2O_5$  occurs only after 90 min of annealing in oxygen ambient. However, annealing does not affect the strong (00 $l$ ) texture of the films. From this, it can be concluded that the conversion of  $V_6O_{13}$  to  $V_2O_5$  is topotactic, consistent with the crystallographic similarities between the two phases.

#### IV. DISCUSSION

Preferred crystallographic orientation in thin films grown on smooth, amorphous substrates has been previously reported.<sup>30</sup> This has been explained to be a consequence of the tendency for minimization of the surface energy of the film.<sup>26,27</sup> Growth occurs in such a way that the most densely packed crystallographic plane of the film material is parallel to the substrate. This reduces the surface energy, leading to strongly textured growth.<sup>30–32</sup> As noted already, the  $a$ - $b$  planes of both  $V_2O_5$  and  $V_6O_{13}$  are made up of networks of corner-sharing octahedra, forming closely packed, dense planes. The strong (00 $l$ ) texture of the  $V_2O_5$  and  $V_6O_{13}$  films deposited on the smooth surface of fused quartz, at temperatures in the range 560–610 °C, may be understood on the basis of

the similarly anisotropic crystal structures of the two oxides. In general, the presence of even a small percentage of a second phase can hinder the development of the microstructure (especially, texture) of the primary phase of a film. However, in the present case, the presence of  $V_2O_5$  in  $V_6O_{13}$  (or vice versa) does not affect the oriented nature of the film because of the similar arrangement of the polyhedra in the two phases in the  $a$ - $b$  plane. This is evident from the SAED patterns (Fig. 5) of  $V_2O_5$  and  $V_6O_{13}$  crystallites taken along [002].

The changing phase content of the films deposited at 10 °C intervals in the range 550 to 590 °C may be represented as  $(V_2O_5 + V_4O_9 + V_6O_{13}) \rightarrow (V_2O_5 + V_6O_{13}) \rightarrow (V_6O_{13} + V_2O_5) \rightarrow (V_2O_5 + V_6O_{13}) \rightarrow (V_2O_5 + V_6O_{13})$ , where the bold font designates the phase dominating the XRD pattern. Between 560 and 580 °C, the phase content displays what may be termed a “reentrant-type” behavior, with  $V_2O_5$  and  $V_6O_{13}$  being the dominant phase by turn, as illustrated schematically in Fig. 9. This may be understood from the close relationship between the crystal structures of  $V_2O_5$  and  $V_6O_{13}$ . As noted in the introduction, the structural similarities between the two oxide phases imply that the difference between their free energies is likely to be small. This is manifest in the binary phase diagram of the V–O system, wherein the phases  $V_2O_5$  and  $V_6O_{13}$  adjoin each other.<sup>6</sup> The existence of vanadium in adjacent oxidation states (the  $V^{5+}$  state in  $V_2O_5$  and both the  $V^{4+}$  and  $V^{5+}$  states in  $V_6O_{13}$ ), and the



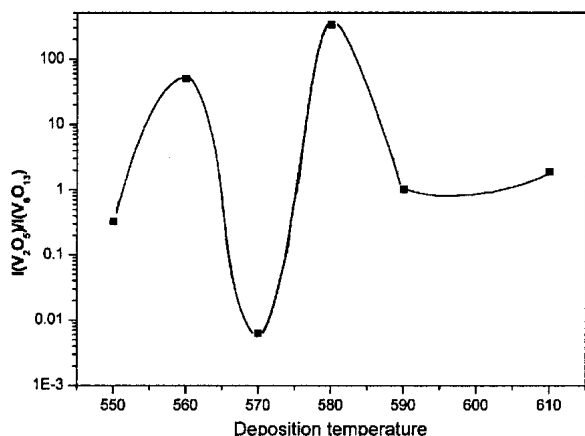


FIG. 9. Variation with growth temperature of the ratio of the intensity of the (001) peak of  $V_2O_5$  to the intensity of the (003) peak of  $V_6O_{13}$ , the strongest of the respective XRD patterns. The solid line is as drawn as a guide to the eye, to illustrate the reentrant-type behavior in the growth of the dominant phase.

close resemblance between their crystal structures, suggests a rather facile interconvertibility between  $V_2O_5$  and  $V_6O_{13}$  through oxidation/reduction. Indeed, such reversible conversion between  $V_2O_5$  and  $V_6O_{13}$  in single-crystal samples has been demonstrated.<sup>6</sup> This is also confirmed here, by the complete topotactic conversion of  $V_6O_{13}$  present in the films V560, V570, and V580 to  $V_2O_5$ . Furthermore, as the metalorganic precursor used in this work,  $VO(acac)_2$ , contains direct V–O bonds in its molecular structure, the binary V–O phase diagram may only be useful as a rough guide to the formation of different oxides of vanadium in the MOCVD process. Given this and the complexity of the low-pressure CVD process, it may be expected that certain deposition conditions may lead to “straggling” across the “phase boundary” that demarcates regions of stability of the two vanadium oxide phases in the binary V–O phase diagram. This can account for the simultaneous deposition of vanadium oxide films deposited at different temperatures in the range 550 to 590 °C, wherein more than one oxide phase is present in each of the films. That the structures of the phases  $V_4O_9$ ,  $V_6O_{13}$ , and  $V_2O_5$  have common features<sup>6</sup> make simultaneous deposition more probable, because the free energies of these oxides may be expected to be close to one another. A similarly simultaneous deposition of two oxide phases of cobalt,  $CoO$  and  $Co_3O_4$ , has been observed<sup>33</sup> in the MOCVD process employing a  $\beta$ -diketonate precursor of Co that contains direct Co–O bonds. Such a simultaneous deposition of two oxides of the same (transition) metal may be rationalized on the basis of thermodynamic modeling of the MOCVD process assuming that equilibrium conditions prevail during the deposition.<sup>34</sup>

The reentrant-type behavior seen in the development of the XRD patterns of the films as a function of deposition temperature may be understood as follows. It is to

be recalled that the thickness of the films deposited at 560 and 570 °C is sharply lower than that of the film deposited at 550 °C. This reduction in thickness is accompanied by the development of a strong crystallographic texture in the films. At 560 °C, the XRD pattern is dominated by  $V_2O_5$ , with a strong (001) texture whereas at 570 °C, the phase  $V_6O_{13}$  with the same (001) texture dominates. As described above [Fig. 3(c)], the film deposited at 570 °C essentially consists of large ( $\sim 20 \mu\text{m}$ ) platelets of  $V_6O_{13}$  covering the entire fused quartz substrate, with much smaller needlelike crystallites with a bright contrast “sprinkled” on the platelets. It is therefore surmised that, at this growth temperature, the conditions are almost exactly those needed for the nucleation and growth of  $V_6O_{13}$ , to the near exclusion of  $V_2O_5$ . Similarly, the growth conditions at 560 °C are close to those needed for the near-exclusive formation of  $V_2O_5$ . As a result of the near exclusion of one of the two phases in the films deposited at 560 and 570 °C, the thickness of the films deposited at these two temperatures is substantially smaller than the thickness of films deposited at neighboring temperatures, either higher or lower (Table I). The films grown at 560 and 570 °C, therefore, represent the formation of nearly pure phases, with a strong (001) texture, attributable to growth on smooth amorphous (silica) substrates, and to the characteristically similar crystal structures of  $V_2O_5$  and  $V_6O_{13}$ . That a difference of 10 °C in the growth temperature (i.e., a difference of 10 K at  $\sim 850$  K) can lead to such a sharp change in the phase content and the microstructure of the films illustrates the closeness of the free energies of these two oxide phases of vanadium. Though striking, such “straggling” across phase boundaries, leading to unusual behavior of the type reported here, is a characteristic of the MOCVD process employing  $\beta$ -diketonate precursors that contain direct metal-oxygen bonds. This is especially so with a multi-valent 3d metal such as vanadium, which forms a rich variety of oxides, including those with ordered defect structures, as well as a number of oxide polymorphs (of  $VO_2$ ) with the same nominal valence.<sup>25</sup>

The domination of the XRD pattern of the film grown at 580 °C by (001)-oriented  $V_2O_5$  probably has a different origin. It must be noted that, at this temperature, the film thickness is sharply higher than that at 560 and 570 °C, suggesting that significant proportions of both  $V_2O_5$  and  $V_6O_{13}$  might have been deposited. However, a close examination of the SEM micrograph [Fig. 3(d)] of this film shows crystallites, which are much more strongly faceted than in other films. As these faceted crystallites have a bright contrast, and as the XRD pattern of this film is dominated by  $V_2O_5$ , it is surmised that the high intensity of the (001) reflections of  $V_2O_5$  arises from the very strong faceting of its crystallites, rather than from the exclusion of the  $V_6O_{13}$  phase altogether.

The absence of a strong (00 $l$ ) orientation in V550 is striking because the structure of  $V_4O_9$  is also similar to those of  $V_2O_5$  and  $V_6O_{13}$  in the  $a$ - $b$  plane. However, a temperature lower by 10 °C may make a crucial difference in “placing” the deposition process in a regime less suitable to the formation of a dominant phase. Moreover, the lower temperature may also provide marginally lower mobility than required for the formation of a strong (00 $l$ ) texture.

At the end of the deposition process, the films were allowed cool down from the deposition temperature under the flow of oxygen (which was maintained). During this cooling, because of the oxygen available, the single crystalline platelets of  $V_6O_{13}$  relax into the thermodynamically more stable oxide,  $V_2O_5$ . However, a complete transformation of the film (the platelets) does not occur, as the natural cooling of the CVD system rapidly brings the deposition chamber to temperatures too low for the oxidation of the edges into  $V_2O_5$  to continue. This incomplete oxidation of  $V_6O_{13}$  accounts for the complex SAED pattern of the platelet edge (Fig. 8), which possibly consists of regions comprising  $V_4O_9$  and  $V_3O_7$ , in addition to  $V_2O_5$ . It is very probable that the extreme edge is made of  $V_2O_5$ . The anisotropy of the crystal structure of  $V_2O_5$  [Fig. 1(c)], with relatively wide “channels” parallel to the  $a$ - $b$  plane, leads to preferred diffusion of oxygen parallel to the  $a$ - $b$  plane, i.e., parallel to the surface of the substrate. As such, oxidation of  $V_6O_{13}$  into  $V_2O_5$ , initiated at the edges, proceeds inwards from the edges of the platelets in a direction parallel to the substrate surface. That is, once the edges of the  $V_6O_{13}$  platelets are oxidized to (or, relax into)  $V_2O_5$ , these transformed edges of the platelets become preferred channels for the diffusion of oxygen, promoting the further oxidation of the “interior” of the platelets. Because of the low rate of oxygen diffusion perpendicular to the  $a$ - $b$  plane of the  $V_6O_{13}$  platelets, the large flat faces of these platelets (parallel to the substrate) are not affected by the oxygen flow during the cool-down. This is evidenced not only by the dark contrast of the platelet faces, but also by the SAED pattern of the “interior” of a platelet, as shown in Fig. 8.

The hypothesis of the relaxation of the platelets of  $V_6O_{13}$  into  $V_2O_5$  is supported by the occurrence of small crystallites “sprinkled” on the platelets of V570. It is observed that, while some of these small crystallites have a fully bright contrast, some are bright at the edges, with the relatively small “interior” region retaining the dark contrast (Fig. 7). As the perimeter-to-volume ratio is high for a small  $V_6O_{13}$  platelet, the diffusion of oxygen into it is greater, leading to the oxidation of a comparatively large proportion of it into  $V_2O_5$ . Indeed, some platelets of  $V_6O_{13}$  relax fully into  $V_2O_5$ . As these  $V_2O_5$  crystallites, too, have the (00 $l$ ) orientation, the XRD pattern of V570 contains (00 $l$ ) reflections due to  $V_2O_5$ , much weaker than

those due to  $V_6O_{13}$ . The proposed hypothesis is further supported by the differing durations of annealing required for the complete (topotactic) conversion of the samples V560, V570, and V580. While a 20-min anneal sufficed to convert V560 and V580 to  $V_2O_5$ , an annealing duration of as much as 90 min was required to convert V570 completely into  $V_2O_5$ . (Such conversion into  $V_2O_5$  was confirmed by the determination of the optical bandgap at 2.0 eV, which corresponds closely to that of  $V_2O_5$ . These converted films were too resistive for R versus T measurements.) This difference in the annealing times required is consistent with the higher proportion of  $V_6O_{13}$  present in V570, necessitating a longer annealing duration for complete oxidation. Furthermore, as noted above, the diffusion of oxygen occurs preferentially along the plane parallel to the substrate, in which direction the crystallite dimension is large (~20  $\mu$ m) compared to its dimension perpendicular to the substrate surface (~0.5  $\mu$ m, the film thickness).

It is likely that the sample V570, as deposited, comprised entirely of  $V_6O_{13}$ . To have retained the integrity of the monophasic sample, it would have been necessary to cool the sample down not in flowing oxygen, but in an appropriate buffering mixture of gases (such as  $H_2/H_2O$ ). In such a mixture, the oxygen partial pressure varies as a function of temperature in such a way as to be consistent with the maintenance of the integrity of the desired phase.<sup>35</sup> However, a detailed, accurate binary V:O phase diagram would be needed to choose the correct buffering gas mixture, given the narrow range of stability of a phase such as  $V_6O_{13}$ .

The transformation of the edges of the single crystalline platelets of  $V_6O_{13}$  to semiconducting  $V_2O_5$ , detailed above, can account for the observed electrical behavior of V570. Even though the film is made of well-connected platelets of  $V_6O_{13}$ , the connection takes place between adjacent platelets at their edges, which have relaxed into  $V_2O_5$ . (The electrical behavior of  $V_3O_7$  and  $V_4O_9$  is not known. We assume that they are semiconducting, just as  $V_2O_5$ .) Thus, the metallic behavior of  $V_6O_{13}$  observed in single crystals is suppressed in the film V570, even though it is made of highly oriented single crystalline platelets of  $V_6O_{13}$ . However, the M-S transition in  $V_6O_{13}$  is evidenced in the change in slope of the Arrhenius plot of the resistance of V570 (Fig. 6). The resistivity of V570 at low temperatures is complex, and may be attributed to the intricate composition of the edges of the platelets, as established by TEM.

Based on this understanding of the electrical behavior of the film V570 that is predominantly made of  $V_6O_{13}$ , we have attempted to interpret the reported<sup>3</sup> electrical properties of sintered, polycrystalline  $V_6O_{13}$ . The semiconducting nature of this specimen at room temperature is likely to have been due to the relaxation of the surface of the pellet (during cool-down) to  $V_2O_5$ , to which

electrical contacts are effectively made. However, the interior of the pellet probably remained metallic  $V_6O_{13}$ . Given that the pellet was 0.3 mm thick, and assuming a thin outer layer of  $V_2O_5$ , the temperature dependence of the conductivity of this composite may be expected to show a very small  $E_a$ , in contrast with reported<sup>3</sup> value at room temperature of 0.42 eV. As this is much larger than the  $E_a = 0.07$  eV measured in V570 at room temperature, we examined the conductivity versus temperature data of Kachi et al.<sup>3</sup> and computed the  $E_a$  using these data. The value of  $E_a$  is found to be 0.02 eV at room temperature, and 0.01 eV at low temperatures. These much smaller values are consistent with our hypothesis that the sintered pellet of Kachi et al.<sup>3</sup> consisted of metallic  $V_6O_{13}$  enveloped in an ostensibly thin outer layer of  $V_2O_5$ , formed due to relaxation during the cooling of the pellet after it was sintered. The re-computed  $E_a$  of this sintered pellet at low temperature (0.01 eV) is consistent with the value of  $E_a$  (~0.03 eV) calculated from the data of Kawashima et al.<sup>2</sup> for single-crystalline  $V_6O_{13}$  below the M-S transition temperature. This supports the conjecture that the surface of the pellet had relaxed into  $V_2O_5$ , within which the bulk of the metallic  $V_6O_{13}$  was embedded.

## V. SUMMARY AND CONCLUSIONS

Strongly (00 $l$ )-oriented composite films of  $V_2O_5$  and  $V_6O_{13}$  have been grown on fused quartz at temperatures  $\geq 560$  °C by MOCVD. Such textured growth stems from the tendency for minimization of interfacial energy when growth occurs on a smooth, amorphous substrate. Films grown below 560 °C are composed of a mixture of  $V_2O_5$ ,  $V_6O_{13}$ , and  $V_4O_9$ , with no tendency for any preferred orientation. When the growth temperature is increased from 560 to 580 °C in steps of 10 °C, a reentrant-type behavior in the dominant phase of the film alternating between  $V_2O_5$  and  $V_6O_{13}$  is observed, as evidenced by XRD and RBS analyses. Such a growth trend is related to the close relationship between the crystal structures of  $V_2O_5$  and  $V_6O_{13}$ , which, in turn, is reflected in the proximity of the two oxide phases on the binary V–O phase diagram. It is proposed that the intriguing reentrant-type growth stems also from the nature of the growth process that employs a precursor with built-in V–O bonds. These factors combine to make the range of conditions in which either pure  $V_2O_5$  or pure  $V_6O_{13}$  is deposited extremely narrow, rendering the formation of a thin film composite of the two phases more probable than not. Resistance measurements of the film dominated by strongly oriented and highly connected single crystalline platelets of  $V_6O_{13}$  show no evidence for S-M transition known to occur in single crystals of  $V_6O_{13}$  at 150 K. Instead, the film undergoes a semiconductor-to-semiconductor (S-S) transition. This may be understood from the (unintended)

oxidation of the edges of  $V_6O_{13}$  platelets to  $V_2O_5$  during the cool-down to room temperature, as observed by SEM and confirmed by TEM. As such, the platelets of metallic  $V_6O_{13}$  are in fact connected to one another through semi-conducting  $V_2O_5$ , suppressing the S-M transition, and resulting in a S-S transition. The transformation of the edges to  $V_2O_5$  is the result of the relaxation of crystallites of  $V_6O_{13}$  into the thermodynamically more stable  $V_2O_5$ , which occurs during the postdeposition cooling of the films to room temperature. Such a relaxation/transformation explains the previously reported observation of a S-S transition in polycrystalline  $V_6O_{13}$  material, rather than a S-M transition. Indeed, the electrical data on our thin films help reconcile the measurements on sintered  $V_6O_{13}$ . The topotactic conversion of all samples into (00 $l$ )-oriented  $V_2O_5$  through post-deposition annealing in oxygen is consistent with these observations. The results presented here, therefore, point to the importance of controlling the conditions under which oxide films and oxide ceramics are cooled from their formation temperature, and has implications for the stability of the composition and properties of transition metal-containing films/fine particles, because of their large surface area/volume ratio. Thus, the present study presents a coherent picture of the close relationship between the binary phase diagram of a transition metal–oxygen system, and the CVD of thin films of the oxides of the metal from precursors containing metal–oxygen bonds.

## ACKNOWLEDGMENTS

The authors are grateful to G. Ananthakrishna for very useful discussions and a careful reading of the manuscript. The authors acknowledge the assistance provided by the late G.N. Subbanna in the TEM analysis of the samples, and V. Jayaram in the interpretation of the microscopy data. The authors wish especially to thank Sanjiv Kumar for the RBS analysis of the films. MBS thanks the Council of Scientific Industrial Research, New Delhi, for a senior research fellowship.

## REFERENCES

1. I. Hevesi, L.B. Kiss, M.I. Torok, and L. Nanai: Electron concentration in vanadium(V) oxide single crystals as determined by 1/f noise measurements. *Phys. Status Solidi, Appl. Res. A* **81**, K67 (1984).
2. K. Kawashima, Y. Ueda, K. Kosuge, and S. Kachi: Crystal growth and some electric properties of  $V_6O_{13}$ . *J. Cryst. Growth* **26**, 321 (1974).
3. S. Kachi, T. Takada, and K. Kosuge: Electrical conductivity of vanadium oxides. *J. Phys. Soc. Jpn.* **18**, 1839 (1963).
4. I. Kawada, M. Nakano, M. Saeki, M. Ishii, N. Kimizuka, and M. Nakahira: Phase transition of vanadium oxide ( $V_6O_{13}$ ). *J. Less-Common Met.* **32**, 171 (1973).
5. A.C. Gossard, F.J. Di Salvo, L.C. Erich, J.P. Remeika, H. Yasuoka, K. Kosuge, and S. Kachi: Microscopic magnetic properties of

- vanadium oxides: II.  $V_3O_5$ ,  $V_5O_9$ ,  $V_6O_{11}$ , and  $V_6O_{13}$ . *Phys. Rev. B* **10**, 4178 (1974).
- J. Haber, M. Witko, and R. Tokarz: Vanadium pentoxide I. Structures and properties. *Appl. Catal. A: General* **157**, 3 (1997).
  - R. Enjalbert and J. Galy: A refinement of the structure of vanadium pentoxide. *Acta Crystallogr. C* **42**, 1467 (1986).
  - R. De Gryse, J.P. Landuyt, A. Vermeire, and J. Vennik: A combined LEIS (low energy ion scattering)-LEED study of the  $V_6O_{13}(001)$  surface. *Appl. Surf. Sci.* **6**, 430 (1980).
  - V.I. Parvulescu, S. Boghosian, V. Parvulescu, S.M. Jung, and P. Grange: Selective catalytic reduction of NO with  $NH_3$  over mesoporous  $V_2O_5$ - $TiO_2$ - $SiO_2$  catalysts. *J. Catal.* **217**, 172 (2003).
  - Z. Huang, Z. Zhu, Z. Liu, and Q. Liu: Formation and reaction of ammonium sulfate salts on  $V_2O_5/AC$  catalyst during selective catalytic reduction of nitric oxide by ammonia at low temperatures. *J. Catal.* **214**, 213 (2003).
  - S. Zhuiykov, W. Wlodarski, and Y. Li: Nanocrystalline  $V_2O_5$ - $TiO_2$  thin-films for oxygen sensing prepared by sol-gel process. *Sens. Actuators B* **77**, 484 (2001).
  - S. Passerini, A.L. Tipton, and W.H. Smyrl: Spin coated  $V_2O_5$  XRG as optically passive electrode in laminated electrochromic devices. *Sol. Energy Mater. Sol. Cells* **39**, 167 (1995).
  - J.M. McGraw, C.S. Bahn, P.A. Parilla, J.D. Perkins, D.W. Readey, and D.S. Ginley: Li ion diffusion measurements in  $V_2O_5$  and  $Li(Co_{1-x}Al_x)O_2$  thin-film battery cathodes. *Electrochim. Acta.* **45**, 187 (1999).
  - M.E. Garcia, E. Webb III, and S.H. Garofalini: Molecular dynamics simulation of  $V_2O_5/Li_2SiO_3$  Interface. *J. Electrochem. Soc.* **145**, 2155 (1998).
  - G.J. Fang, Z.L. Liu, Y.Q. Wang, H.H. Liu, and K.L. Yao: Oriented growth of  $V_2O_5$  electrochemic thin films on transparent conductive glass by pulsed excimer laser ablation technique. *J. Phys. D: Appl. Phys.* **33**, 3018 (2000).
  - J.M. McGraw, J.D. Perkins, F. Hasoon, P.A. Parilla, C. Warmsingh, and D.S. Ginley: Pulsed laser deposition of oriented  $V_2O_5$  thin films. *J. Mater. Res.* **15**, 2249 (2000).
  - D. Barreca, L. Armelao, F. Caccavale, V.D. Noto, A. Gregori, G.A. Rizzi, and E. Tondello: Highly oriented  $V_2O_5$  nanocrystalline thin films by plasma-enhanced chemical vapour deposition. *Chem. Mater.* **12**, 98 (2000).
  - T.D. Manning, I.P. Parkin, R.J.H. Clark, D. Sheel, M.E. Pemble, and D. Vernadou: Intelligent window coatings: atmospheric pressure chemical vapour deposition of vanadium oxides. *J. Mater. Chem.* **12**, 2936 (2002).
  - A.M. Abo El Soud, B. Mansour, and L.I. Soliman: Optical and electrical properties of  $V_2O_5$  thin films. *Thin Solid Films* **247**, 140 (1994).
  - S. Kobayashi, T. Takemura, and F. Kaneko: Dependence of absorption in electrochromic  $V_2O_5$  thin films on crystallinity. *Jpn. J. Appl. Phys.* **26**, L1274 (1987).
  - M.Z.A. Munshi, W.H. Smyrl, and C. Schmidtke: Insertion reaction of  $V_6O_{13}$  electrodes reversibly incorporating divalent cations. *Solid State Ionics* **47**, 265 (1991).
  - J.S. Braithwaite, C.R.A. Catlow, J.H. Harding, and J.D. Gale: A theoretical study of lithium intercalation into  $V_6O_{13}$ -a combined classical, quantum mechanical approach. *Phys. Chem. Chem. Phys.* **3**, 4052 (2001).
  - A. Gorenstein, A. Khelfa, J.P. Guesdon, G.A. Nazri, O.M. Hussain, I. Ivanov, and C. Julien: The growth and electrochemical properties of  $V_6O_{13}$  flash-evaporated films. *Solid State Ionics* **76**, 133 (1995).
  - X.J. Wang, H.D. Li, Y.J. Fei, X. Wang, Y.Y. Xiong, Y.X. Nie, and K.A. Feng: XRD and Raman study of vanadium oxide thin films deposited on fused silica substrates by RF magnetron sputtering. *Appl. Surf. Sci.* **177**, 8 (2001).
  - M.B. Sahana, M.S. Dharmaprakash, and S.A. Shivashankar: Microstructure and properties of  $VO_2$  thin films deposited by MOCVD from vanadyl acetylacetonate. *J. Mater. Chem.* **12**, 333 (2002).
  - M.B. Sahana, G.N. Subbanna, and S.A. Shivashankar: Phase transformation and semiconductor-metal transition in thin films of  $VO_2$  deposited by low-pressure metalorganic chemical vapor deposition. *J. Appl. Phys.* **92**, 6495 (2002).
  - M.B. Sahana and S.A. Shivashankar: Growth of nanowires of  $\beta$ - $Na_xV_2O_5$  by metalorganic chemical vapor deposition. *J. Mater. Chem.* **13**, 2254 (2003).
  - Joint Committee on Powder Diffraction Standards (JCPDS) Powder Diffraction File (PDF) database, published annually by the International Centre for Diffraction Data, USA.
  - N. Kenay, O.R. Kannewurf, and D.H. Whitmore: Optical absorption coefficients of vanadium pentoxide single crystals. *J. Phys. Chem. Solids* **27**, 1237 (1966).
  - J-G. Yoon, H.K. Oh, and S.J. Lee: Growth characteristics and surface roughening of vapor-deposited MgO thin films. *Phys. Rev. B* **60**, 2839 (1999).
  - C.V. Thompson and H.I. Smith: Surface-energy-driven secondary grain growth in ultrathin (<100 nm) films of silicon. *Appl. Phys. Lett.* **44**, 603 (1984).
  - H.I. Smith and D.C. Flanders: Oriented crystal growth on amorphous substrates using artificial surface-relief gratings. *Appl. Phys. Lett.* **32**, 349 (1978).
  - A.U. Mane and S.A. Shivashankar: MOCVD of cobalt oxide thin films: Dependence of growth, microstructure, and optical properties on the source of oxidation. *J. Cryst. Growth* **254**, 368 (2003).
  - K. Shalini: Development and Application of Metalorganic Complexes as Precursors for the Chemical Vapor Deposition of Oxide Thin Films. Ph.D. Thesis, Indian Institute of Science, Bangalore, India, 2002.
  - P. Deines, R.H. Nafziger, G.C. Ulmer, and E. Woerman: Temperature-oxygen fugacity tables for gas mixtures in system C-H-O at one atmosphere total pressure. *Bulletin of Earth and Minerals Experimental Section*, No. 88 (The Pennsylvania State University, University Park, PA, 1974).